

# Magnetic Resonance Studies of Trapping Centers in High- $\kappa$ Dielectric Films on Silicon

Patrick M. Lenahan, *Member, IEEE*, and John F. Conley, Jr., *Senior Member, IEEE*

*Invited Paper*

**Abstract**—The electrical properties of high dielectric constant materials being considered for replacements of SiO<sub>2</sub> in metal-oxide semiconductor (MOS) field effect transistors are dominated by point defects. These point defects play important roles in determining the response of these films in almost any imaginable reliability problem. A fundamental understanding of these defects may help to alleviate the problems which they can cause. The best known methods for determining the structure of electrically active defects in MOS materials and devices are conventional electron spin resonance (ESR) and electrically detected magnetic resonance (EDMR). In this paper, we review the limited ESR and EDMR work performed to date on high- $\kappa$  materials. A discussion of magnetic resonance techniques as well as a brief overview of the extensively studied Si/SiO<sub>2</sub> system is also included.

**Index Terms**—Defects, electron paramagnetic resonance (EPR), electron spin resonance (ESR), gate insulator, high dielectric constant, high- $\kappa$ , MOS, reliability, trapping.

## I. INTRODUCTION

THE International Technology Roadmap for Semiconductors [1] indicates that the currently used gate dielectric materials will be insufficient to sustain the aggressive scaling of metal-oxide-semiconductor (MOS) devices that has enabled the microelectronics industry to follow Moore's Law for over thirty years. These ultrathin films based on SiO<sub>2</sub> and its nitrated derivatives (Si-O-N) exhibit excessive gate leakage current which can lead to extremely high power dissipation. A solution to this problem may be the use of high dielectric constant materials which would allow a physically thicker, but capacitively equivalent material to be used as the gate dielectric [2]. Early on, Hubbard and Schlom [3] identified certain binary oxides as thermodynamically stable on silicon while Robertson [4] calculated bandgaps and offsets for a variety of oxides. As a result, most interest has focused on Al<sub>2</sub>O<sub>3</sub>, ZrO<sub>2</sub>, and HfO<sub>2</sub>, as candidates to replace SiO<sub>2</sub>. All exhibit lower leakage currents than SiO<sub>2</sub> at equivalent oxide thickness. HfO<sub>2</sub> and ZrO<sub>2</sub> both have higher dielectric constants ( $\kappa \approx 25$ ) than Al<sub>2</sub>O<sub>3</sub> ( $\kappa < 9$ ). However, HfO<sub>2</sub> is favored over ZrO<sub>2</sub> because it is more stable

against silicide formation than ZrO<sub>2</sub> [5]. For these and other reasons, HfO<sub>2</sub> based dielectrics are widely considered to be the most promising high- $\kappa$  candidates.

There are several major challenges in the integration of high- $\kappa$  gate dielectric materials in MOS systems. A critical requirement for any potential high- $\kappa$  gate dielectric replacement for SiO<sub>2</sub> is the quality of the Si/dielectric interface [2]. Many groups report electrical measurements of interface trap density,  $D_{it}$ , in the range of  $\sim 10^{11} - 10^{12}/\text{cm}^2 \text{ eV}$ , a density much higher than that observed in device quality Si/SiO<sub>2</sub>. In addition to high  $D_{it}$ , many groups report high densities ( $\geq 10^{12}/\text{cm}^2$ ) of shallow electron traps in HfO<sub>2</sub>/Si films [6]–[10]. Our results on atomic layer deposited (ALD) HfO<sub>2</sub> films indicated quite high densities ( $> 2 \times 10^{12} \text{ cm}^{-2}$ ) of large capture cross section electron traps and also indicated that some trapped electrons stay trapped over long periods of time [6]. Electron trapping was also observed in similar samples subject to constant voltage stress [7]. A recent study by Zafar *et al.* [8] reported positive threshold voltage shifts in ALD HfO<sub>2</sub> gate n-field effect transistor devices, resulting from high electric field stressing. They argued that the trapping of charges occurred at existing traps, and that their experimental procedure did not create additional traps. Zhu *et al.* [9] recently reported positive flatband voltage shifts which they attribute to negative effective-trapped charge in jet vapor deposited HfO<sub>2</sub> films; they reported a trapped electron density saturating at  $\sim 2 \times 10^{12} \text{ cm}^{-2}$  for all samples in their study. Early on, Gusev *et al.* [10] reported high electron trap densities in HfO<sub>2</sub> based transistors. They found that at low stress voltages, electrons fill existing traps, with creation of new traps being observed at higher stress voltages.

Electron traps and interface traps impact mobility in high- $\kappa$  devices. The fact that some electron traps can rapidly charge and discharge and that trap generation takes place at high fields but not at low fields makes reliability assessment (accelerated testing and lifetime extrapolation) extremely difficult, posing a possible fundamental physical limit for high- $\kappa$  dielectric based transistors as discussed in other papers in this special issue. Very little is known about the atomic scale structure of the electrically active defects responsible for trapping in these high- $\kappa$ /Si systems. Understanding the origin and physical nature of high- $\kappa$ /Si interface traps and bulk trapping centers will be crucial in developing an interface comparable to that of SiO<sub>2</sub>. Magnetic resonance methods such as conventional electron spin resonance (ESR) and electrically detected magnetic resonance (EDMR)

Manuscript received November 24, 2004; revised January 18, 2005. The work at Penn State was sponsored by Intel Corporation through Semiconductor Research Corporation Custom Funding.

P. M. Lenahan is with the Pennsylvania State University, University Park, PA 16802 USA.

J. F. Conley, Jr., is with the Sharp Laboratories of America, Camas, WA 98607 USA (e-mail: jconley@sharplabs.com).

Digital Object Identifier 10.1109/TDMR.2005.845475

are the best techniques currently available for understanding the structure of these point defects.

After a brief review of the ESR and EDMR measurement techniques, this work reviews magnetic resonance investigations of interface and dielectric trapping defects in Si/high- $\kappa$  systems. For a basis of comparison, a brief overview of the extensive work on SiO<sub>2</sub>/Si systems is provided.

## II. MAGNETIC RESONANCE MEASUREMENTS: THEORY AND OPERATION

### A. Electron Spin Resonance

A schematic of an ESR spectrometer is shown in Fig. 1. In ESR, the sample is placed in a microwave cavity that is critically coupled to a microwave generator. The cavity is placed between the pole faces of a magnet which supplies a large magnetic field,  $H$ . In order to make a measurement, the magnetic field is slowly swept with the microwave frequency,  $\nu$  held constant. If defects with unpaired electrons are present, resonance will occur at magnetic field determined by the structure of the defect and the orientation of this defect within the magnetic field. In conventional ESR, resonance is observed by monitoring the net absorption of microwave power by the sample; the absorption changes the coupling of the cavity, reflecting microwave power back through the circulator to be measured by detector electronics. In order to improve sensitivity and signal to noise, a small oscillating magnetic field is superimposed on the large magnetic field and a lock-in amplifier is used. Signal averaging often provides an additional improvement in signal to noise. Although only defects with unpaired electrons can be detected, in principle, essentially any electrically active defect may be placed into an ‘‘ESR active’’ state through capture of either an electron or a hole.

By making comparisons with a calibrated spin standard, the amount of power absorbed at resonance allows determination of defect concentrations. Defect concentration measurements are typically accurate to better than a factor of two in absolute number and about  $\pm 10\%$  in relative number. For most of the studies reviewed in this paper, ESR samples consist of a thin film of dielectric on a high resistivity Si substrate. Typically the samples are not coated with a metal or poly-Si gate. More than one sample may be stacked in an ESR cavity to improve signal to noise.

Information about the local environment or structure of the defect can be gleaned from the relationship between the magnetic field and microwave frequency at which resonance occurs, known as the  $g$  tensor. In the simplest cases, the  $g$  is defined by

$$g = \frac{h\nu}{\beta H} \quad (1)$$

where  $h$  is Planck’s constant,  $\nu$  is the microwave frequency,  $\beta$  is the Bohr magneton, and  $H$  is the magnetic field at which resonance is observed. The  $g$  tensor can be related to the electron wave function through a second order perturbation theory calculation:

$$g_{ij} = g_0\delta_{ij} + 2\lambda \sum_k \frac{\langle d|L_i|k\rangle\langle k|L_j|d\rangle}{(E_k - E_d)} \quad (2)$$

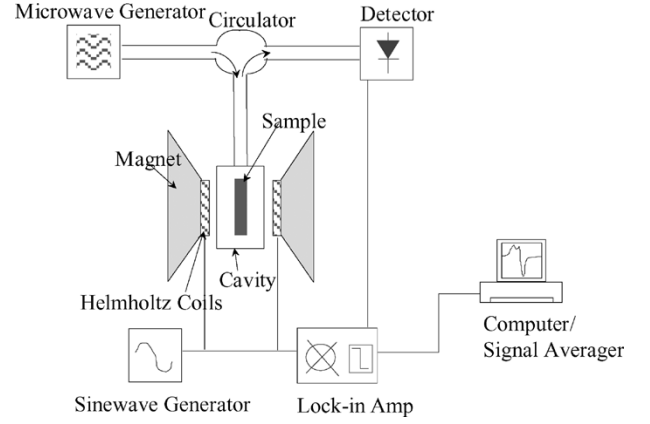


Fig. 1. Schematic of an ESR system.

Here  $\lambda$  is the atomic spin orbit coupling constant,  $g_0 = 2.00232$  is the free electron  $g$ -value,  $L_i$  and  $L_j$  are angular momentum operators defined with respect to the  $i$  and  $j$  directions of the defect’s principal axis system,  $d$  represents the defect ground state electron wave function,  $k$  corresponding to the other possible states, and  $E$  energy levels. The  $g$  is dependent on the magnetic field vector and its relationship to the defect’s principal axis system. The symmetry of the  $g$  tensor reflects the symmetry of the paramagnetic defect center under study.

The ESR  $g$  value of an axially symmetric defect (most of the defects discussed in this paper have axial or near axial symmetry) is given by

$$g = (g_{\parallel}^2 \cos^2 \theta + g_{\perp}^2 \sin^2 \theta)^{\frac{1}{2}} \quad (3)$$

where  $g_{\perp}$  corresponds to the tensor value for the magnetic field parallel (perpendicular) to the defect axis of symmetry.

Additional information about the structure of paramagnetic defects can be obtained from observations of the interaction of unpaired electrons with magnetic nuclei; these are called hyperfine interactions. About 5% of silicon nuclei are magnetic <sup>29</sup>Si which possess a nuclear spin  $-1/2$ . Nearly 100% of hydrogen and nitrogen nuclei are magnetic; most hydrogen possess a spin  $1/2$  nucleus and most nitrogen have spin  $-1$  nuclei. The limited conventional ESR and EDMR studies of high dielectric constant thin films have yet to exploit observation of electron nuclear hyperfine interactions; however, observation of electron nuclear hyperfine interactions was quite useful in developing an understanding of deep level centers in conventional SiO<sub>2</sub> based MOS technology. As is the case in the observation of spin orbit interactions, electron nuclear hyperfine interactions are described in terms of a second rank tensor.

### B. Electrically Detected Magnetic Resonance

EDMR or spin dependent recombination (SDR), is very similar to ESR but the detection scheme involves measurements of spin dependent changes in device currents. Instead of a capacitor-like test structure, EDMR typically utilizes a working MOS transistor configured as a gate controlled diode. Instead of measuring microwave power absorption, a resonance induced change in recombination current is monitored. As very small

changes in current can be measured with a highly sensitive electrometer, the sensitivity of this technique is many orders greater than that standard ESR. EDMR does not directly provide a quantitative measurement of defect density, though qualitative differences can be readily inferred.

### III. OVERVIEW OF MAGNETIC RESONANCE STUDIES OF THE Si/SiO<sub>2</sub> SYSTEM

Extensive magnetic resonance studies have provided a first order understanding of trapping defects at the Si/SiO<sub>2</sub> interface and in the SiO<sub>2</sub> “bulk.” To set the stage for the discussion of high- $\kappa$  results, a brief overview of the major results is included here. More extensive reviews of ESR in MOS systems can be found elsewhere [11], [12].

#### A. Si/SiO<sub>2</sub> Interface Defects

Beginning with the work of Nishi, *et al.* [13], and later extended and expanded by several other groups [14]–[21] the dominant electrically active defects at the Si/SiO<sub>2</sub> interface have been identified as several varieties of P<sub>b</sub> centers (P<sub>b</sub>, P<sub>b0</sub>, P<sub>b1</sub>). All P<sub>b</sub> centers consist of an unpaired electron on a Si back-bonded to three other Si atoms at the Si/SiO<sub>2</sub> interface. Initial measurements by Nishi *et al.* [13] and later, more extensive, measurements by Poindexter and coworkers [14], [15] linked P<sub>b</sub> densities to the densities of interface traps in Si/SiO<sub>2</sub> capacitors of relatively low quality, that is in capacitors with fairly high to high as-processed interface trap density. Lenahan and coworkers [16]–[21] and later other groups established similar relationships between P<sub>b</sub> densities and interface traps generated in high quality devices via a number of device reliability problems such as radiation damage, hot carrier stressing, high oxide field stressing, etc..

Measurements of several groups established that the P<sub>b</sub> centers have two levels in the silicon bandgap [16], [17], [22], [23]. The essentially identical (111) Si/SiO<sub>2</sub> P<sub>b</sub> centers and (100) Si/SiO<sub>2</sub> P<sub>b0</sub> centers each have two (fairly broad) levels separated by about 0.7 eV and more or less symmetrically distributed in the silicon band gap. The (100) Si/SiO<sub>2</sub> P<sub>b1</sub> variant has two levels separated by just a few tenths of an electron volt, with the density of states is skewed toward the lower part of the silicon bandgap [24]. The most important of the P<sub>b</sub> centers is the P<sub>b0</sub> center; it generally dominates conventional technologically relevant (100) Si/SiO<sub>2</sub> interface instability problems [18], [19], [21]. A schematic of a (100) P<sub>b0</sub> center is shown in Fig. 2. A  $g$ -tensor map (plot of  $g$  value versus angle) from Kim, *et al.* [18] is shown in Fig. 3. The  $g$ -map is constructed by making ESR measurements at various orientations of the sample in the magnetic field. The solid lines in Fig. 3 were fit using (3) and indicate that for the (100) Si interface P<sub>b0</sub>,  $g_{\parallel} = 2.0013$  and  $g_{\perp} = 2.008$ . <sup>29</sup>Si hyperfine by Gabrys, *et al.* [21] provided a more detailed picture of P<sub>b0</sub> structure, clearly demonstrating that the P<sub>b0</sub> center involves an unpaired electron in a very high p-character wave function strongly localized on a single silicon. Recent <sup>29</sup>Si hyperfine measurements by Stesmans *et al.* [25] confirmed the Gabrys *et al.* results of a P<sub>b0</sub> and furthermore provided a more definitive identification of the P<sub>b1</sub> center which also involves a (100) Si/SiO<sub>2</sub> interface silicon “dangling bond”

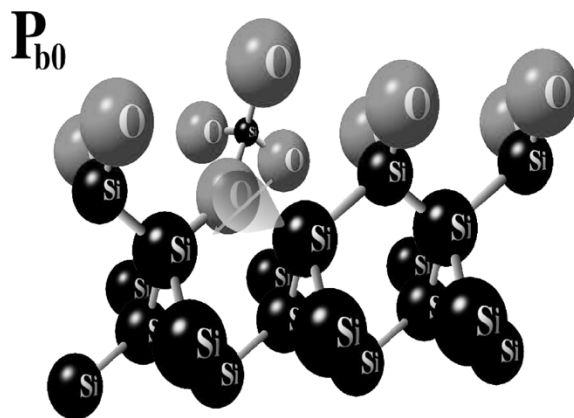


Fig. 2. Illustration of the P<sub>b0</sub> center, the most important conventional (100) Si/SiO<sub>2</sub> interface trapping center. Quite similar defects clearly play important roles in new high dielectric constant/silicon based devices.

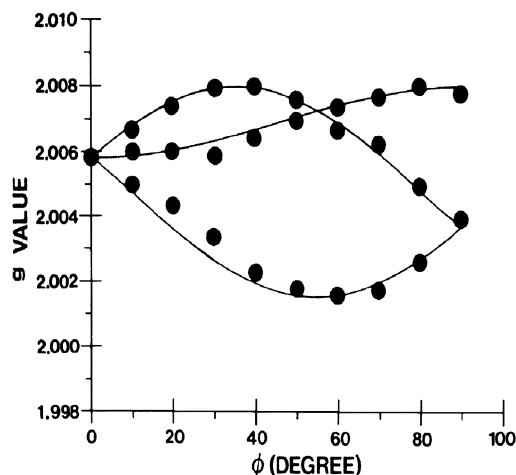


Fig. 3. Plot of  $g$ -value versus angle for P<sub>b0</sub> in which the angle is defined by the difference between the (100) Si/interface normal and magnetic field. The sample is rotated about the (110) axis. From Kim *et al.* [18].

center in which the unpaired electron is also rather highly localized in a high p-character orbital on an Si/SiO<sub>2</sub> interface silicon atom.

#### B. SiO<sub>2</sub> “Bulk” Intrinsic Defects

By far, the most significant family of defects in SiO<sub>2</sub> are known as E' centers. These defects involve an unpaired electron residing on a silicon back-bonded to three oxygens. The most widely studied E' center is an oxygen vacancy in the SiO<sub>2</sub> consisting of an unpaired electron on a Si atom that is back-bonded to three O atoms. A schematic of this E' center variant is shown in Fig. 4. Early studies in the 1980's showed that these defects are the dominant hole traps in SiO<sub>2</sub> [17], [18], [26], a result that was confirmed in numerous subsequent studies [27]–[32]. E' center variants have been shown to dominate <sup>60</sup>Co and VUV irradiation [17], [18], [26]–[31], [33]–[35], low field stressing, and SOI buried oxides. E' centers have also been implicated in reliability problems such as time dependent dielectric breakdown [36], [37] and SILC [38]. A predictive thermodynamics based model of E' center precursor density in thermally grown SiO<sub>2</sub> was proposed by Lenahan and Conley, *et al.* [39]–[42].

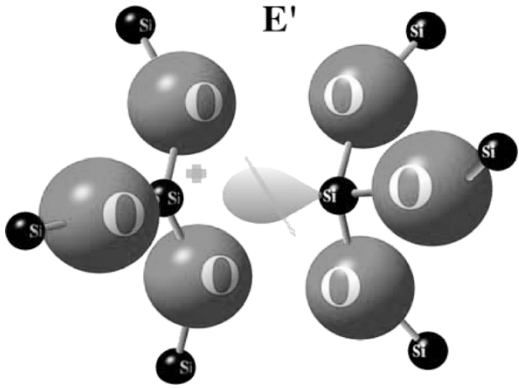


Fig. 4. Illustration of an  $E'$  center variant. The  $E'$  center family dominates the electronic properties of conventional  $\text{SiO}_2$  gate oxides. This  $E'$  variant is a hole trapped in an oxygen vacancy.

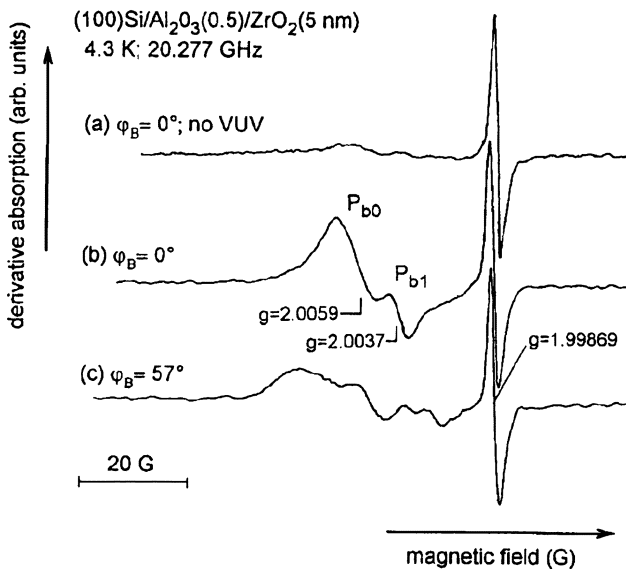


Fig. 5.  $P_{b0}$  and  $P_{b1}$  defect spectrums, in a stacked  $\text{Si}/\text{Al}_2\text{O}_3/\text{ZrO}_2$  structure. From Stesmans and Afanas'ev [44].

#### IV. REVIEW OF MAGNETIC RESONANCE STUDIES OF $\text{Si}/\text{HIGH-}\kappa$ SYSTEMS

##### A. Interface of $\text{Si}/\text{High-}\kappa$ Systems

The first ESR study of the interface of a  $\text{Si}/\text{high-}\kappa$  system was conducted by Stesmans and Afanas'ev [43], [44]. A dielectric stack consisting of  $(100)\text{Si}$  (HF last)/ $0.5\text{ nm Al}_2\text{O}_3/5\text{ nm ZrO}_2$  was investigated.  $\text{Al}_2\text{O}_3$  and  $\text{ZrO}_2$  were deposited via atomic layer deposition (ALD) using either tri-methyl aluminum (TMA) and  $\text{H}_2\text{O}$  or  $\text{ZrCl}_4$  and  $\text{H}_2\text{O}$ . ESR measurements were taken at  $4.3\text{ K}$  and  $20.277\text{ GHz}$ . As-deposited samples show very weak signals. After  $8.48\text{ eV}$  vacuum ultraviolet illumination, ESR spectra (shown in Fig. 5) similar to  $\text{Si}/\text{SiO}_2$   $P_{b0}$  and  $P_{b1}$  centers were detected. A  $g$ -map for these defects is shown in Fig. 6. Their analysis of the  $g$ -tensor [using (3)] yields  $g_{\parallel} = 2.00185$  and  $g_{\perp} = 2.0081$  for  $P_{b0}$  and  $g_1 = 2.00577$ ,  $g_2 = 2.00735$ , and  $g_3 = 2.0022$  for  $P_{b1}$ , which the authors argue is, in both cases, within experimental error, identical to that observed in  $\text{Si}/\text{SiO}_2$ . The signals appear to be broadened in comparison to the  $\text{Si}/\text{SiO}_2$  signals, which the authors suggest is due to low quality  $\text{SiO}_2$ . The authors interpret their results as an indication that the  $\text{Si}/\text{high-}\kappa$  interface is identical to a low quality  $\text{Si}/\text{SiO}_2$  interface.

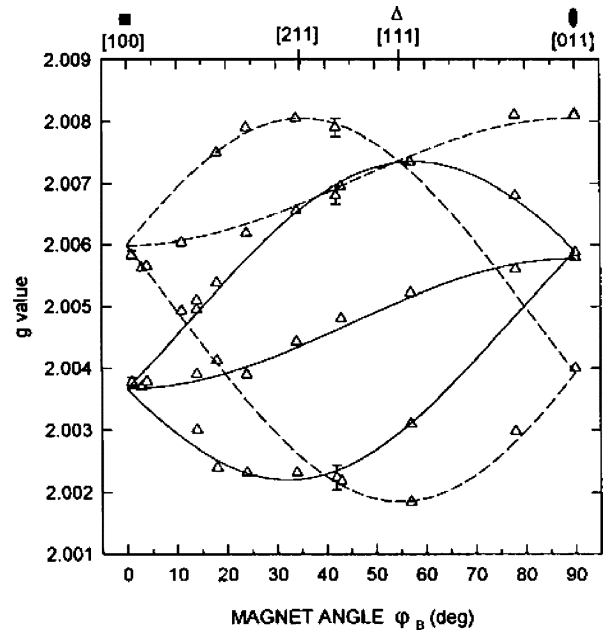


Fig. 6.  $G$ -map of  $P_{b0}$  and  $P_{b1}$  center spectra taken on a stacked  $\text{Si}/\text{Al}_2\text{O}_3/\text{ZrO}_2$  structure. Here, the angle  $\varphi$  is defined as the difference between the  $(100)$   $\text{Si}/\text{interface}$  normal and the magnetic field. The sample is rotated about the  $(110)$  axis. From Stesmans and Afanas'ev [43].

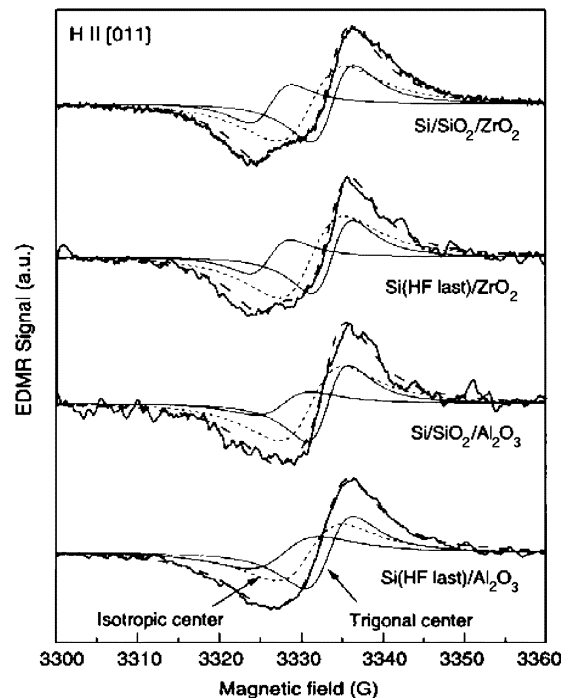


Fig. 7. EDMR traces of  $\text{ZrO}_2$  and  $\text{Al}_2\text{O}_3$  based devices. From Baldovino, *et al.* [45].

$\text{Si}/\text{ZrO}_2$  and  $\text{Si}/\text{Al}_2\text{O}_3/\text{Si}$  interfaces were investigated by Baldovino *et al.* [45] using spin dependent photoconductivity EDMR. In their room temperature measurements, samples were exposed to  $470\text{ nm}$  light and the spin dependent change in photoconductivity was measured.  $\text{ZrO}_2$  films ( $15\text{ nm}$  thick) and  $\text{Al}_2\text{O}_3$  films ( $11\text{ nm}$  thick) were grown via ALD using either TMA and  $\text{H}_2\text{O}$  or  $\text{HfCl}_4$  and  $\text{H}_2\text{O}$ , respectively.  $\text{Si}$   $(100)$  surface preparation prior to ALD was either HF last or native oxide. As shown in Fig. 7, they found comparable levels of

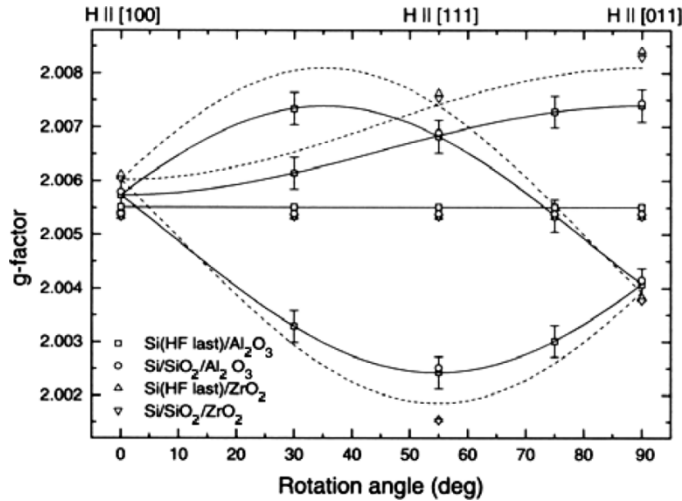


Fig. 8.  $g$ -map for data from Fig. 7. Dashed lines are Stesmans *et al.* data. The rotation angle is the angle between the (100) Si/dielectric surface normal and the magnetic field. The rotation is about the (110) axis. From Baldovino *et al.* [45].

$P_{b0}$ -like defects in all samples. Analysis of their  $g$ -tensor, shown in Fig. 8, yields  $g_{\parallel} = 2.0024$  and  $g_{\perp} = 2.0074$  for  $P_{b0}$  in  $ZrO_2$  and  $g_{\parallel} = 2.0016$  and  $g_{\perp} = 2.0084$  for  $P_{b0}$  in  $Al_2O_3$ . The  $g$ -values extracted for  $ZrO_2$  are similar for both HF-last and native oxide surfaces and are similar to those reported for  $SiO_2$ . As it is well known that ALD growth of  $ZrO_2$  or  $HfO_2$  on HF-last (H-terminated) Si using  $ZrCl_4$  or  $HfCl_4$  results in poor initiation and growth of a rough interfacial layer [7], [46]–[48], this result suggests growth of an  $SiO_x$  interfacial layer. The  $g$  values extracted for  $Al_2O_3$  are significantly different than those reported for  $SiO_2$ , suggesting an interface distinctly different from  $Si/SiO_2$ .

The first magnetic resonance studies of  $HfO_2$  films on silicon were initiated by Kang *et al.* [49]–[51]. Kang *et al.* investigated  $HfO_2$  films with a combination of ESR and electrical measurements.  $HfO_2$  films were deposited on H-terminated (111) and (100) Si by ALD using  $Hf(NO_3)_4$  and  $H_2O$  as precursors [7], [52], [53].  $HfO_2$  samples were 14.5 nm thick and had an interfacial layer thickness of 0.5–1.2 nm. High resistivity substrates and relatively thick films without a metal or poly capping layer were used to improve ESR sensitivity. The use of (111) Si substrates [49]–[51] follows the approach of early ESR work on  $Si/SiO_2$ , taking advantage of the simpler surface structure where all the Si bonds are oriented in the  $\langle 111 \rangle$  direction [11], [13], [14]. Low resistivity (100) Si substrates were used for electrical measurements. Capacitor structures were formed either by evaporating Pt using a shadow mask, or photolithographic patterning of TiN. ESR measurements were made at room temperature at 150 K operating at X-band. Fig. 9 shows ESR traces taken with the magnetic field parallel to (a) and perpendicular to (b) the (111) surface normal. The spectra clearly reveal the presence of several defects. One of these defects, the strongest signal in Fig. 9, is identified by arrows in both parts (a) and (b). This signal has  $g$  tensors parameters deduced from the  $g$  map of Fig. 10:  $g_{\parallel} = 2.0018$  and  $g_{\perp} = 2.0094$ . The axis of symmetry for this defect, the  $\langle 111 \rangle$  axis, also can be deduced, where the  $g$  value versus the angle between the magnetic field orientation and the  $\langle 111 \rangle$  axis of the Si substrate is mapped out.

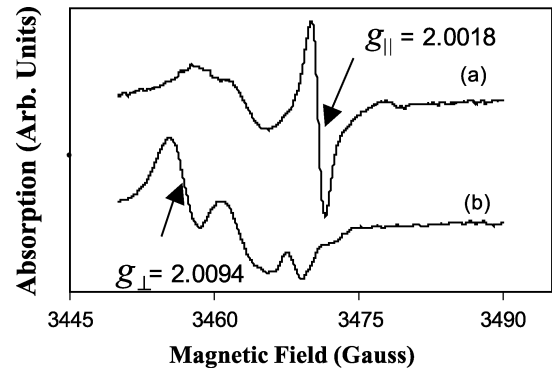


Fig. 9. ESR traces of  $HfO_2/(111)Si$  sample with magnetic field (a) parallel to and (b) perpendicular to the (111) surface normal. The  $HfO_2$  interface silicon dangling bond defect is designated by arrows in parts (a) and (b). From Kang *et al.* [49].

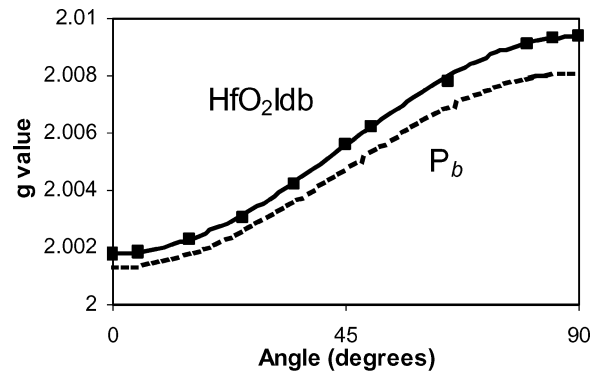


Fig. 10. ESR  $g$ -value anisotropy map for the  $HfO_2$  interface silicon dangling bond defect on (111) silicon substrate at different values of angle rotation of the magnetic field. The solid line is given by the equation (3) with  $g_{\parallel} = 2.0018$  and  $g_{\perp} = 2.0094$ . The dashed line is the same equation with  $g_{\parallel} = 2.0013$  and  $g_{\perp} = 2.0081$  for the (111)  $Si/SiO_2$   $P_b$  dangling bond defect. From Kang *et al.* [50].

The  $g$  tensor values of this signal ( $g_{\parallel} = 2.0018$  and  $g_{\perp} = 2.0094$ ) are similar to but not the same as those of the (111)  $Si/SiO_2$   $P_b$  interface dangling bond ( $g_{\parallel} = 2.0013$  and  $g_{\perp} = 2.0081$ ). Both have the same (111) symmetry axis. They attributed this signal to a  $P_b$ -like silicon dangling bond at the interface of the  $HfO_2/Si$  system. However, the fact that the differences between the  $g$  tensor of the  $HfO_2/Si$   $P_b$ -like dangling bond and that of the  $SiO_2/Si$  interface  $P_b$  dangling bond are much larger than experimental error, demonstrates that for these H-terminated Si substrates, the  $HfO_2/Si$  interface dangling bond is somewhat different, consistent with electrical and TEM measurements. Shown in Fig. 11 is a plot of capacitive equivalent thickness versus optical thickness for a series of ALD  $HfO_2$  films [54]. If one assumes that the interfacial layer is independent of film thickness, extrapolation of a linear fit to the data in this figure intersects the y axis at about 0.7 nm, suggesting an interfacial layer with an equivalent electrical thickness of 0.7 nm. Shown in Fig. 12(b) is a TEM image of a similarly deposited 5 nm thick ALD  $HfO_2$  film clearly showing an interfacial layer thickness of 1.1–1.2 nm [48]. The fact that the physical thickness of the interfacial layer is greater than its electrical thickness indicates that the interfacial layer has  $k > 3.9$  and is thus not pure  $SiO_2$ . If the interfacial layer were pure  $SiO_2$ , one would expect that the observed  $g$  tensor values would be

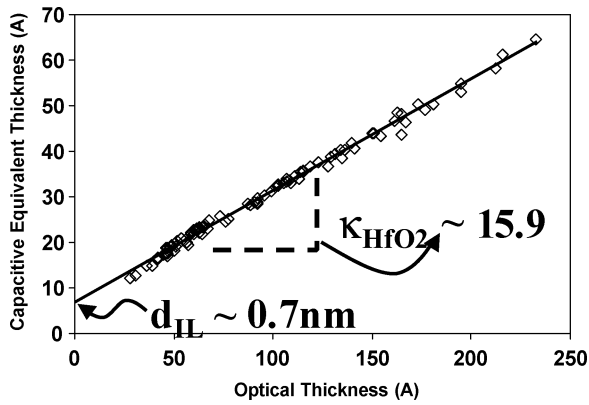


Fig. 11. Plot of capacitive equivalent thickness versus optical thickness for a series of ALD  $\text{HfO}_2$  films. From Conley, *et al.* [54].

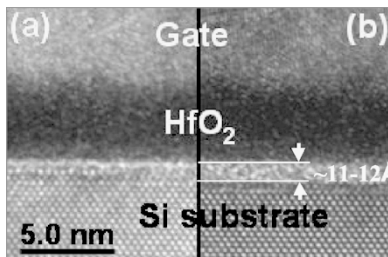


Fig. 12. TEM image of (a) an ALD  $\text{HfO}_2$  film deposited using dual metal precursors and modulated temperature annealing (MTA) and (b) an ALD  $\text{HfO}_2$  film deposited without MTA. The image in (b) clearly shows an interfacial layer thickness of 1.1–1.2 nm. The addition of modulated temperature annealing in (a) allows a reduction of interfacial thickness to  $\sim 0.5$ – $0.6$  nm. From Conley *et al.* [48].

identical to those of the  $\text{Si}/\text{SiO}_2$   $P_b$  center; this is clearly not the case.

Figs. 13 and 14 suggest close links between the interface dangling bonds and interface traps in the  $\text{HfO}_2/\text{Si}$  system. Fig. 13 compares ESR spectra of  $\text{HfO}_2/(111)\text{Si}$  samples for (a) as processed and (b) post-60 second  $400^\circ\text{C}$  forming gas ( $5\% \text{H}_2/95\% \text{N}_2$ ) anneals. A 70% decrease in the ESR signal intensity corresponds to the CV curves in Fig. 14 which show a clear decrease in  $N_{it}$ .

ESR studies in conventional  $\text{SiO}_2/\text{Si}$  on (100) silicon substrates demonstrated that the (111) studies were relevant to the problems at hand, as an essentially identical defect dominates both interfaces [14], [18]. If the  $\text{Si}/\text{SiO}_2$  analogy holds for the  $\text{HfO}_2/\text{Si}$   $P_b$  like defect structures, (3) predicts that a single  $\text{HfO}_2/(100)$  Si silicon dangling bond signal with  $g = 2.0069$  would be observed for a magnetic field oriented along the (100) surface normal ( $\theta = 54.7^\circ$ ), if, as is the case for the (111) interface,  $g_{||} = 2.0018$  and  $g_{\perp} = 2.0094$ . This prediction is confirmed in Fig. 15, in which ESR measurements on (100)  $\text{Si}/\text{HfO}_2$  samples reveal that the strongest signal present appears at the predicted  $g$  value,  $g = 2.0068 \pm 0.0002$ . The conventional (100)  $\text{Si}/\text{SiO}_2$   $P_{b0}$  signals would be  $g = 2.0059$  for this orientation.

In a later study by Stesmans and Afanas'ev [55],  $\text{HfO}_2$  films (5–7 nm thick) deposited via three different methods were investigated. Shown in Fig. 16 are post 8.48 eV photo-dissociation ESR traces of  $\text{HfO}_2$  samples deposited via either ALD ( $300^\circ\text{C}$ ,  $\text{HfCl}_4$  &  $\text{H}_2\text{O}$ ), metal-organic chemical vapor deposition (MOCVD,  $485^\circ\text{C}$ , TDEAH &  $\text{O}_2$ ), or CVD ( $350^\circ\text{C}$ ,

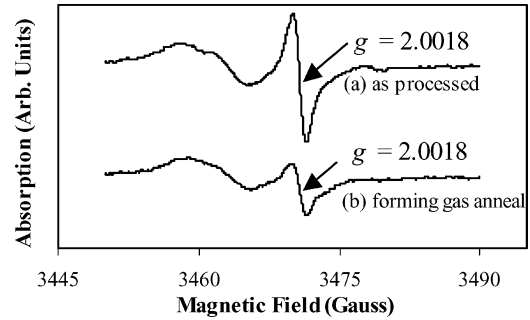


Fig. 13. ESR spectra of the (a) as processed and (b) post 60 sec  $400^\circ\text{C}$  forming gas anneal sample of the ALD  $\text{HfO}_2/(111)\text{Si}$  system. The sharp peak in the middle of the spectra corresponds to the  $\text{HfO}_2$  interface silicon dangling bond defect. The forming gas anneal reduced the dangling bond signal by 70%. From Kang, *et al.* [49].

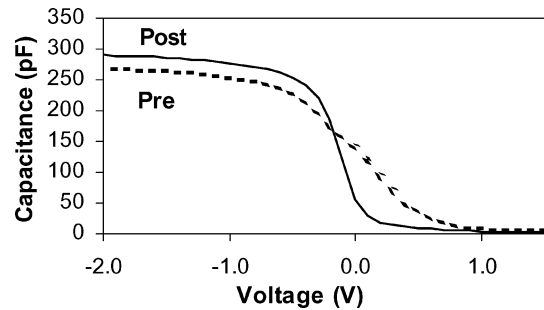


Fig. 14. 1 MHz Capacitance versus voltage traces of a  $\sim 147\text{Å}$  thick  $\text{HfO}_2$  film, before (Pre) and after (Post) a 60 sec,  $400^\circ\text{C}$  anneal in forming gas. From Kang, *et al.* [49].

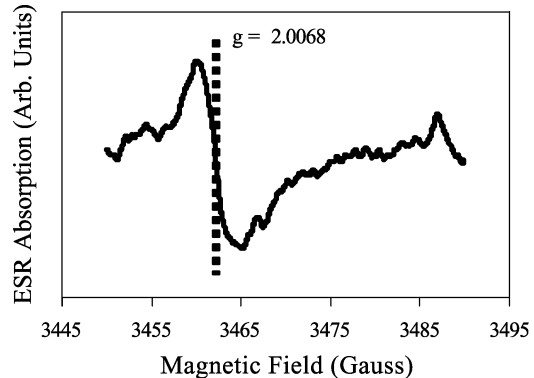


Fig. 15.  $\text{HfO}_2/(100)$  Si silicon interface dangling bond signal with  $g = 2.0069$  for a magnetic field oriented along the (100) surface normal. Adapted from Kang, *et al.* [50].

$\text{Hf}(\text{NO}_3)_4$ ). ESR traces were taken at 4.3 K and 20.5 GHz. They find that the density of  $P_{b0}$ -like and  $P_{b1}$ -like defects is process dependent. ALD and MOCVD samples show  $P_{b0}$  and  $P_{b1}$  densities of approximately  $2 \times 10^{12}/\text{cm}^2$  each while the CVD film shows about four times higher  $P_{b0}$  density.  $P_{b0}$  and  $P_{b1}$  can be passivated by a  $400^\circ\text{C}$  forming gas anneal and reduced by oxygen anneals. Although no  $g$ -tensor analysis was reported for these samples, the authors conclude that the observed  $P_{b0}$  and  $P_{b1}$  signals are identical to those observed at the  $\text{Si}/\text{SiO}_2$  interface and suggest that the interfacial layer does not contain Hf but may be O deficient.

Finally, Lenahan *et al.* [56], recently found another defect at the  $\text{HfO}_2/\text{Si}$  boundary in a sub-set of samples. Fig. 17 shows

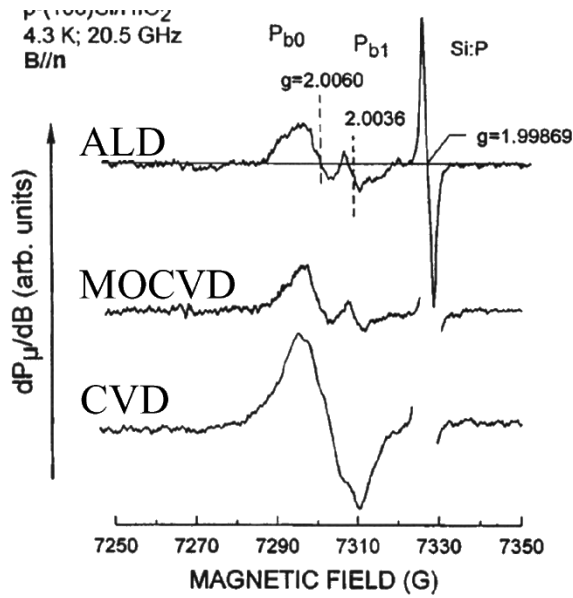


Fig. 16. ESR traces taken with the magnetic field perpendicular to the (100) Si/dielectric interfaces. Adapted from Stesmans and Afanas'ev [55].

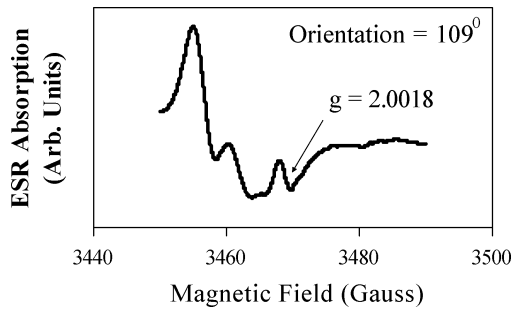


Fig. 17. ESR traces of  $\text{HfO}_2/(111)\text{Si}$  sample with magnetic field oriented  $109^\circ$  from the (111) surface normal. The back-bonded  $\text{HfO}_2$  interface silicon dangling bond defect is designated by the arrow. Adapted from Kang, *et al.* [49].

an ESR trace taken with the magnetic field at an angle of  $109^\circ$  with the (111) surface normal axis. A much weaker signal was detected with  $g$  tensors  $g_{\parallel} = 2.0018$  and  $g_{\perp} \cong 2.009$ . The  $g$  map of the defect (shown in Fig. 18) indicates that this defect has an axis of symmetry pointing  $109^\circ$  from the (111) surface normal. In a tetrahedral bonding arrangement, such as that found in crystalline Si, the bonds are  $109.5^\circ$  apart. Therefore, given its axis of symmetry and practically identical  $g$  tensor values, the signal of Fig. 17 is most likely that of a back-bonded silicon dangling bond as illustrated in Fig. 19.

A very recent EDMR (SDR) study on fully processed  $\text{HfO}_2$  metal gate transistors provides very strong evidence that  $P_b$ -like defects will play important roles in  $\text{HfO}_2$  gate transistor reliability problems. It also directly links  $P_b$ -like centers to interface traps. Pribicko *et al.* [57] observe  $P_b$ -like spectra in SDR measurements. The (100) Si/ $\text{HfO}_2$  transistors utilized in their study had TiN gates. The transistor's nominal 2 nm  $\text{HfO}_2$  gate dielectric (EOT  $\sim 1$  nm) was deposited by ALD using an  $\text{HfCl}_4$  precursor. The interface between the  $\text{HfO}_2$  and the silicon included a nominal 0.4 nm chemical oxide. The key result of their study is illustrated in Fig. 20. As the figure illustrates, oxide electric

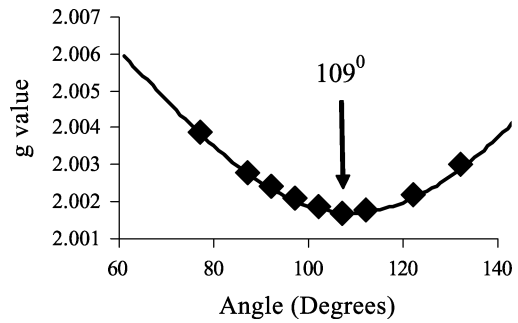


Fig. 18. ESR  $g$ -value anisotropy map for the back-bonded  $\text{HfO}_2$  interface silicon dangling bond defect on (111) silicon substrate at different values of angle rotation of the magnetic field. The solid line is given by the equation (3) with  $g_{\parallel} = 2.0018$  and  $g_{\perp} \cong 2.009$ . From Lenahan *et al.* [56].

field stressing generates significant densities of  $P_b$ -like Si/dielectric interface traps. This increase in  $P_b$ -like defect density is accomplished by an increase in interface trap density, as indicated by the increasing amplitude of the recombination current. The authors [57] also report a hysteretic effect in the interface trap generation process. Application of a sequence of alternating positive and negative gate bias results in respective increases and decreases in the  $P_b$ -like defect SDR amplitudes as well as interface trap density (evaluated via gate controlled diode surface recombination velocity measurements). Their results suggest very strongly that at least partially reversible chemical reactions at the  $P_b$ -like sites are triggered by various gate biases. Their results also clearly indicate that  $P_b$ -like centers can play an important role in high- $\kappa$  dielectric MOS reliability phenomena.

Finally, one other group has also reported (rather low signal to noise ratio) ESR traces of  $P_{b0}$  and  $P_{b1}$ -like defects in (100)Si/ $\text{Al}_2\text{O}_3$  samples [58].  $\text{Al}_2\text{O}_3$  films (4 nm thick) were deposited via ALD using TMA and  $\text{H}_2\text{O}$ .

### B. "Bulk" High- $\kappa$ Defects: Intrinsic

To the best of our knowledge, only one group has used ESR measurements to study intrinsic defects in the bulk of a high- $\kappa$  film.  $\text{HfO}_2$  films deposited on H-terminated Si via ALD ( $\text{Hf}(\text{NO}_3)_4$  &  $\text{H}_2\text{O}$ ) were investigated by Kang, *et al.* [6] with a combination of ESR and electrical measurements. The samples utilized in the ESR portion of the study were 42.7 nm thick and received a  $420^\circ\text{C}$  post deposition  $\text{N}_2$  anneal for 60 seconds. The films were made quite thick to increase the volume of dielectric in the ESR cavity and thereby increase the sensitivity of the measurements. The samples utilized in the CV measurements were 25.7 nm thick, and received a  $450^\circ\text{C}$  post deposition  $\text{N}_2$  anneal for 60 seconds. CV (100 kHz) measurements were made using either a mercury probe to form a temporary gate electrode or on photolithographically defined TiN gate capacitors.

A plot of CV flatband voltage versus electron fluence is illustrated in Fig. 21. A corona ion/UV illumination technique was used to photo-inject charge into  $\text{HfO}_2$  films [59]. The electrons were injected at relatively low average oxide field ( $\leq 2$  MV/cm) and the density of injected electrons was also rather low; thus, it is likely that the observed charge build up is due to trapping at pre-existing defects or defect precursors. With the simplifying assumptions that trap density is uniform

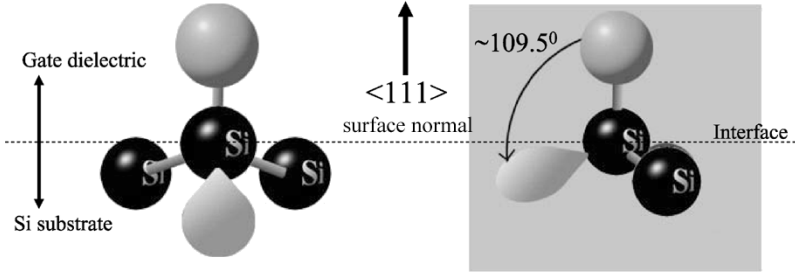


Fig. 19. Schematic illustration of the back-bonded  $\text{HfO}_2$  silicon interface dangling bond defect.

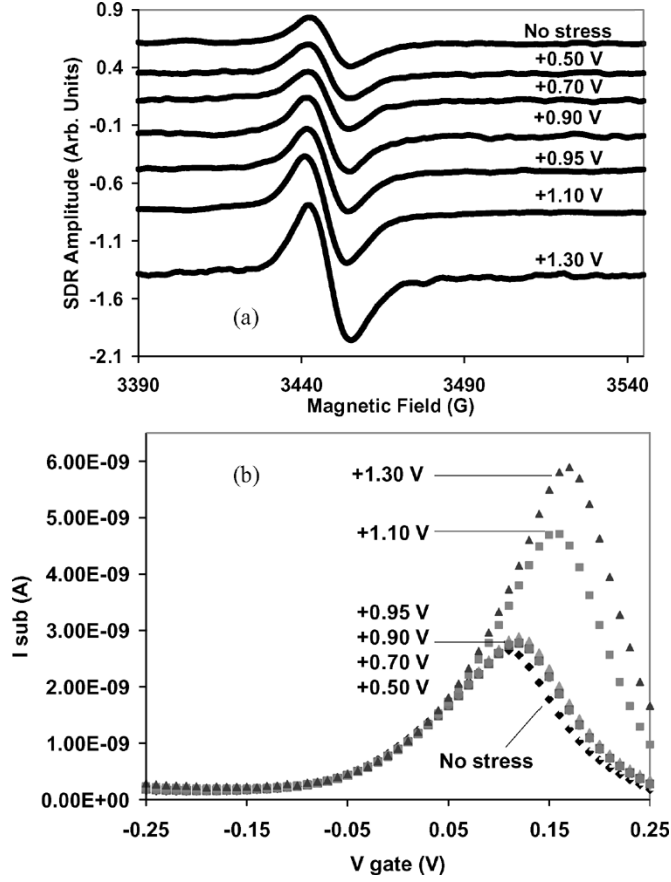


Fig. 20. EDMR measurements on a fully processed metal gate  $\text{HfO}_2$  transistor configured as a gate controlled diode. (a) Comparison of SDR amplitude changes after 30 minute gate voltage stresses. (b) Comparison of gate controlled diode current after 30 minute gate voltage stresses. Note the correspondence between increasing current peaks and SDR amplitudes. From Pribicko *et al.* [57].

throughout the dielectric and that only a single trap capture cross section need be considered, the flatband voltage shift may be described by:

$$\Delta V_{\text{FB}} = \left[ \frac{N_t e}{C_{\text{ox}} 2} \right] (1 - e^{-\sigma \eta}) \quad (4)$$

where  $C_{\text{ox}}$  is the oxide capacitance per unit area,  $N_t$  is the number of traps per unit area,  $e$  is electronic charge,  $\sigma$  the capture cross-section, and  $\eta$  is the fluence (charge carriers injected per unit area). The solid line in Fig. 21 is a plot of the  $\Delta V_{\text{FB}}$  versus fluence as obtained by (4). A fit of (4) to the data in Fig. 21, indicates that  $\Delta V_{\text{FB}}$  versus fluence can be fit to a curve

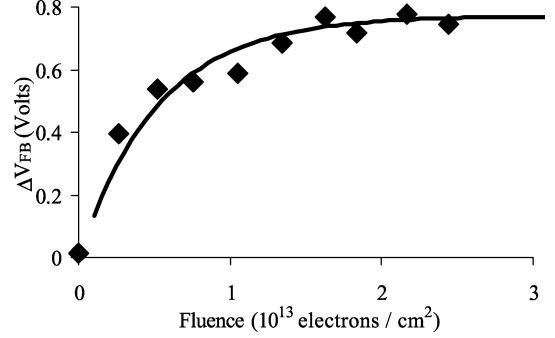


Fig. 21. Flatband voltage shift versus electron fluence for a 25.6 nm ALD  $\text{HfO}_2$  film. The  $\Delta V_{\text{FB}}$  data can be fit to a curve obtained from equation (4) (solid line) with capture cross section  $\sigma$  of  $3 \times 10^{-13} \text{ cm}^2$  and trap density  $N_t$  of  $2 \times 10^{12} \text{ cm}^{-2}$ . From Kang *et al.* [49].

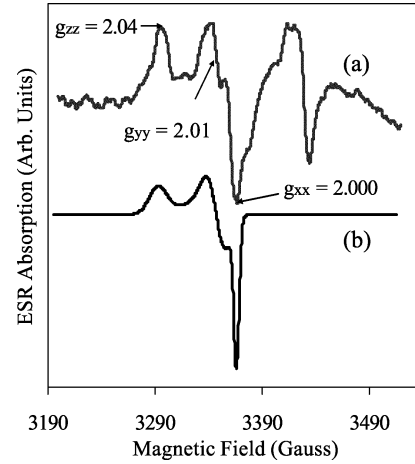


Fig. 22. (a) ESR trace generated by electron photo-injection at an electron fluence of  $2 \times 10^{13} \text{ cm}^{-2}$ . (b) Simulated ESR spectra with  $g_{zz} = 2.04$ ,  $g_{yy} = 2.01$ , and  $g_{xx} = 2.000$ . From Kang *et al.* [6].

corresponding to a capture cross section  $\sigma$  of  $3 \times 10^{-13} \text{ cm}^2$  and trap density of  $N_t = 2 \times 10^{12} \text{ cm}^{-2}$ . These numbers imply simple filling of a large density of pre-existing traps of large capture cross-section.

Fig. 22 illustrates ESR spectra generated by the electron injection. The same electron injection procedure was used for the ESR measurements as for the CV measurements of Fig. 21. However, as mentioned previously, ESR samples were somewhat thicker and were grown on high resistivity substrates to enhance the sensitivity of the ESR measurements. The fairly complex pattern presented in Fig. 22, corresponds to two different center spectra. The  $g$ -tensor for the signal on the left-hand side of Fig. 22(a) is  $g_{zz} = 2.04$ ,  $g_{yy} = 2.01$ ,  $g_{xx} =$

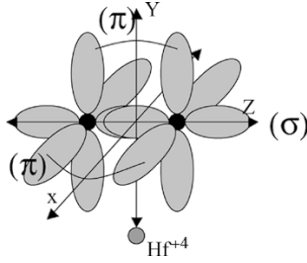


Fig. 23. Schematic diagram of the  $\pi$  wave functions for an  $O_2^-$  molecule defect. From Kang, *et al.* [6].

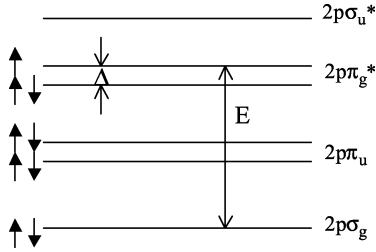


Fig. 24. Electronic energy levels of the  $O_2^-$  defect. From Kang, *et al.* [6].

2.000. A computer simulation<sup>1</sup> of a spectrum expected for a randomly oriented array of defects with this  $g$  tensor is illustrated in Fig. 22(b).

Numerous ESR studies of materials with ionic bond characteristics have identified ESR spectra similar to these, as due to  $O_2^-$  ions coupled to cations [60]–[71]. Kanzig and Cohen [72] have derived expressions for the  $g$  tensor of  $O_2^-$  ion defects, based on the electronic ground state energy levels for the  $O_2^-$  in an ionic system as depicted by Fig. 23. The Kanzig and Cohen model should hold for  $HfO_2$ , since the Hf-O bond has 70% ionic character. As Fig. 23 illustrates, the  $O_2^-$  ion has both  $\sigma$  and  $\pi$  bonding. The crystal field around the defect removes the degeneracy of the  $\pi$  bonding and antibonding levels, splitting the  $2p\pi_g$  orbitals by an energy  $\Delta$ , as shown in Fig. 24. Following the energy level diagram of Fig. 24, Kanzig and Cohen derived the expressions for the  $g$  tensors:

$$g_{xx} = g_e \left( \frac{\Delta^2}{\lambda^2 + \Delta^2} \right)^{\frac{1}{2}} - \frac{\lambda}{E} \left[ - \left( \frac{\lambda^2}{\lambda^2 + \Delta^2} \right)^{\frac{1}{2}} - \frac{\Delta}{(\lambda^2 + \Delta^2)^{\frac{1}{2}}} + 1 \right] \quad (5)$$

$$g_{yy} = g_e \left( \frac{\Delta^2}{\lambda^2 + \Delta^2} \right)^{\frac{1}{2}} - \frac{\lambda}{E} \left[ \left( \frac{\lambda^2}{\lambda^2 + \Delta^2} \right)^{\frac{1}{2}} - \frac{\Delta}{(\lambda^2 + \Delta^2)^{\frac{1}{2}}} - 1 \right] \quad (6)$$

$$g_{zz} = g_e + 2 \left( \frac{\lambda^2}{\lambda^2 + \Delta^2} \right)^{\frac{1}{2}} l \quad (7)$$

where  $g_e = 2.0023$  is the free electron  $g$  value,  $\lambda$  is the spin orbit coupling of oxygen (usually taken to be 0.014). The energy level separations  $E$  and  $\Delta$  are defined in Fig. 24. The parameter  $l$  is

<sup>1</sup>The simulation was carried out using WINEPR SimFonia Simulation Software of Bruker Instruments, Billerica, MA.

a correction to the angular momentum about  $z$  caused by the crystal field and is normally close to one [70]–[72]. In general,  $\lambda < \Delta \ll E$ , and thus to a first order approximation, (5)–(7) may be simplified to yield:  $g_{xx} \cong g_e$ ,  $g_{yy} \cong g_e + 2\lambda/E$ ,  $g_{zz} \cong g_e + 2\lambda/\Delta$ .

Thus,  $g_{xx}$  is usually very close to the free electron  $g = 2.0023$ , and  $g_{yy}$  is generally shifted somewhat higher than the free electron; its value is typically about  $2.01 \pm 0.001$ . As indicated by the simplified (7), the magnitude of the  $g_{zz}$  component is greatly influenced by the local surroundings which result in the crystal field splitting  $\Delta$ , and is thus a good indicator of the environment surrounding the  $O_2^-$  ion. The larger the electronic crystal field present at the defect site, the smaller the deviation of  $g_{zz}$  from the free electron value.

The Kanzig and Cohen model for the  $O_2^-$  ion has been widely accepted in the literature dealing with these centers in many ionic materials [60], [72]. ESR characterization of the  $O_2^-$  ion in ionic materials has been reviewed by Lunsford [70] and Che and Tench [71]. Of particular interest with regard to these observations, ESR measurements of the  $O_2^-$  ion in the chemically very similar  $ZrO_2$  system have been reported by several other groups. The  $g$  tensor which we assign to  $O_2^-$  in  $HfO_2$ ,  $g_{zz} = 2.04$ ,  $g_{yy} = 2.01$ ,  $g_{xx} = 2.000$ , is quite similar to that reported in  $ZrO_2$  [66]–[69]:  $g_{zz} \cong 2.033$ ,  $g_{yy} \cong 2.01$ ,  $g_{xx} \cong 2.003$ . As Zr and Hf are chemically similar, the close similarity between the two tensors provides further strong evidence that the  $HfO_2$  ESR spectra is due to an  $O_2^-$  defect.

Kang, *et al.* [6] also reported the generation of a second strong ESR spectrum with electron injection. The signal on the right-hand side of Fig. 22 has a zero crossing  $g = 1.965$ . This signal, like the  $Hf/O_2^-$ , also consistently appears with the electron injection. The magnitude of the signal does not track precisely with that of the  $O_2^-$  ion signal, although the amplitudes do appear to be roughly correlated. This signal is also quite similar to a signal previously reported in  $ZrO_2$  systems. A signal with a  $g$  tensor of  $g_{||} = 1.978$  and  $g_{\perp} = 1.953$  and zero crossing  $g = 1.953$  has been attributed to a  $Zr^{+3}$  related defect in  $ZrO_2$  [66]–[69], [73]. The close chemical similarity between Hf and Zr suggests that  $Hf^{+3}$  and  $Zr^{+3}$  would have somewhat similar spectra; however, the considerably larger spin orbit coupling constant of Hf would require a fortuitous scaling of crystal fields to yield such similar  $g$  tensors. A plausible identification of this defect would be a paramagnetic oxygen vacancy.

### C. “Bulk” High- $\kappa$ Defects: Extrinsic

To date, only one group has reported on the structure of an extrinsic defect in a thin film high- $\kappa$  dielectric. Stesmans and Afanas'ev [74] recently reported an ESR study of  $HfO_2$  films deposited via either CVD, MOCVD, or ALD. CVD was performed at 350 °C using  $Hf(NO_3)_4$  on HF last Si, MOCVD at 485 °C using tetrakis-diethylaminohafnium and  $O_2$  precursors, and ALD at 300 °C using  $HfCl_4$  and  $H_2O$  on  $SiO_2$ . ESR measurements were performed at 4.3–35 K at 20.3 GHz and 34.9 GHz. As shown in Fig. 25 they observe a three line ESR spectrum in 100 nm thick CVD  $HfO_2$  films. The spectrum appears only after gamma irradiation (50 Mrads) and not after 8.48 eV VUV illumination. An etchback experiment showed that the defects are located in the bulk of the  $HfO_2$  film. They found that

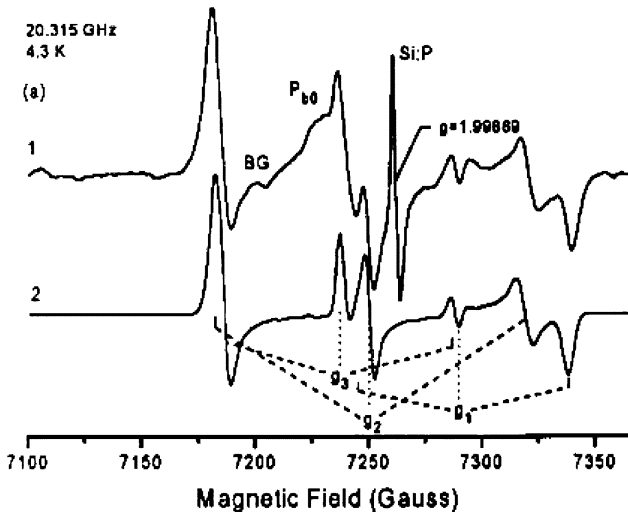


Fig. 25. These traces illustrate paramagnetic  $N_2O$ . Adapted from Stesmans and Afanas'ev [74].

the three lines responded identically to microwave power saturation and could be interpreted with the same set of  $g$  and hyperfine tensors at two different microwave frequencies. The three lines implicate a nuclear spin,  $I = 1$  atom such as  $^{14}N$ . (The nuclear spin of one would yield three possible effective local fields at a defect.) The fact that the defect is only observed in the CVD film, the one deposited using a N-containing precursor, also points to a nitrogen related defect. Based upon these observations, previous ESR literature, and simulations of the line-shape, they assigned the spectra to  $NO_2$  radicals stabilized in the bulk of the  $HfO_2$  film and suggested that the defects could arise due to residual nitrogen from the  $Hf(NO_3)_4$  precursor. XPS results on ALD  $HfO_2$  using  $Hf(NO_3)_4$  as a precursor showed that residual nitrogen groups are left over after deposition and that the nitrogen could be eliminated by a 400 °C anneal [52], [53].

## V. SUMMARY AND DISCUSSION

### A. ESR Results: Si/High- $\kappa$ Interface

1) *Defects:* With respect to defect structures, there is widespread agreement in the ESR high- $\kappa$  literature in that virtually all studies to date report high densities of interfacial Si dangling bond defects at the interface between Si and the high- $\kappa$  stack. These defects clearly involve Si dangling bond centers precisely at the Si/dielectric boundary and are similar (in some cases arguably identical) to the fairly well understood Si/SiO<sub>2</sub>  $P_b$  centers. In addition, the defects respond to forming gas anneals in a manner qualitatively similar to that of the  $P_b$  centers in that their numbers are significantly reduced.

Although the Si/high- $\kappa$  interface experimental magnetic resonance results reported by several groups are similar in broad outline, there is controversy with regard to the detailed conclusions. While some groups argue that the defects at the Si/ZrO<sub>2</sub>, Si/Al<sub>2</sub>O<sub>3</sub>, and Si/HfO<sub>2</sub> interfaces are all identical to the Si/SiO<sub>2</sub> interface [43], [44], [55], [58], other groups conclude that the defects are very similar, but not identical to those observed in conventional SiO<sub>2</sub>/Si devices [45], [49]–[51]. One very possible explanation for the apparent disagreement is simply that these studies involve differently processed films. Processing is

well known to have an impact on both the physical and electrical properties of high- $\kappa$  films, especially for nonoptimized films. For ALD in particular, Si substrate surface preparation is known to have a large impact on the growth and characteristics of the interfacial layer (IL) [46], [47]. So it is quite possible that differences in processing could explain the differences in conclusions.

2) *Reliability Implications:* The electrical behavior of high- $\kappa$  gate stacks is known to be strongly dependent upon the thickness and composition of the IL between the high- $\kappa$  dielectric and the Si substrate. It is also being realized that the details of the IL may be critical for reliability assessment [76].<sup>2</sup> As mentioned above, the thickness and chemical makeup of the IL are strongly dependent upon processing details. Assessment of this 0.5–1.5 nm layer is extremely difficult and thus not much is known about the chemical makeup other than what has been inferred electrically. The ESR studies thus may shed some light on this IL, a region critical to the reliability response of the film. Some ESR studies note interfacial defects somewhat different, though similar to those observed in Si/SiO<sub>2</sub>. Other ESR studies conclude that the interfacial defects are identical to that observed in Si/SiO<sub>2</sub>; these suggest that the IL is pure SiO<sub>2</sub>. However, this is unlikely to be the case in most instances, as comparisons of electrical and TEM measurements indicated that the IL typically has an intermediate dielectric constant. One possible interpretation of identical defects is that the IL could be a poor quality, O-deficient SiO<sub>2</sub>. This is a plausible explanation, as some XPS results indicate the presence of a strained Si rich oxide at the interface and suggest that the O deficiency would result in an increased dielectric constant [75]. Another possibility is that the increased dielectric constant of the IL is due to the presence of some metal (i.e., a silicate). While some EDX/EELS results suggest that silicate formation is unlikely [76], [77], other studies report phase separation at the interface, crystalline high- $\kappa$  and amorphous SiO<sub>2</sub> [75], [78], [79]. The presence of some metal in the IL is consistent with the ESR conclusion that the high- $\kappa$  interface defects are similar, but not identical to, those at the Si/SiO<sub>2</sub> interface.

### B. ESR Results: High- $\kappa$ Bulk

1) *Intrinsic Defects:* Kang *et al.* [6] observed the generation of ESR active defects in ALD HfO<sub>2</sub> due to photo-injection of electrons and noted that the number of trapped electrons is on the order of the density of the defects generated. They concluded that these defects are almost certainly dominating electron trapping centers in the films they studied. The strongest electron trap related defect is that of an O<sub>2</sub><sup>-</sup> center. The density of O<sub>2</sub><sup>-</sup> centers generated by the photo-injection is about  $3 \times 10^{12}/cm^2$ . In addition, they observed a second strong signal (zero crossing  $g = 1.965$ ) as a result of the electron injection, the identity of which is not yet clear, but which may be a paramagnetic O-vacancy. They did note that the signal is similar to one observed in ZrO<sub>2</sub> which has been linked to Zr<sup>+3</sup> ions. Another possible structure is an electron trapped in an oxygen vacancy. The authors conclude that the densities of these intrinsic defects are possibly controllable via processing.

<sup>2</sup>See, for example, other papers in this issue.

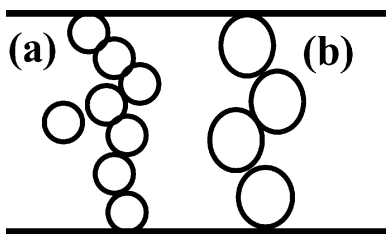


Fig. 26. In percolation theory [90], breakdown causing defects can be modeled as spheres that are randomly generated in the oxide as it is electrically stressed. When enough of these defects line up closely enough and span a dielectric film, breakdown occurs via conduction through this defect path. The bigger the defects are or the greater their sphere of influence, the less defects it should take to produce a breakdown path.

2) *Extrinsic Defect*: Only one extrinsic defect has been reported to date. Stesmans, *et al.* [74] report generation of  $\text{NO}_2$  radicals after 50 Mrads of gamma irradiation. The signal was only observed in  $\text{HfO}_2$  samples that were deposited using a nitrogen containing precursor. Although the electrical properties of this defect were not determined, the study confirms the importance of processing on the properties of high- $\kappa$  films.

3) *Reliability Implications*: Many groups have reported low Weibull slopes in high- $\kappa$  materials that in some cases are independent of thickness [80]–[86]. There are several possible explanations for low Weibull slopes in high- $\kappa$  films. First, it is very likely that at least some of these results were due to extrinsic behavior—the result of poor material quality. However, as film quality has improved Weibull slopes have also increased. Despite this improvement, high- $\kappa$  Weibull slopes are still lower than  $\text{SiO}_2$  films of similar thickness. Polarity also plays a role as under certain bias conditions, and depending on the stack structure, reliability is dominated by the thin IL [82]. Another possibility is nonuniform defect generation, which has been simulated to result in a reduction of Weibull slope [87].

A popular statistical model of breakdown involves percolation theory [88] in which breakdown causing defects can be modeled as spheres that are randomly generated in the oxide as it is electrically stressed. When enough of these defects line up closely enough to span a dielectric film, breakdown occurs via conduction through this defect path. According to percolation theory, the bigger the defects are, or the greater their sphere of influence, the less defects it takes for breakdown to occur and the lower the Weibull slope (see Fig. 26). Percolation theory might imply that the low Weibull slopes reported in high- $\kappa$  films could be due to the smaller number of larger radius traps needed for breakdown in these films [82].

Thus, another possible reason for low Weibull slopes may be due to the nature of defect centers in high- $\kappa$  materials [89]. Due to d-shell based conduction bands [77], the bandgaps of high- $\kappa$  materials are smaller than the bandgap of  $\text{SiO}_2$  which may lead to somewhat more shallow deep levels in these dielectrics. The dominating deep level defect family in conventional  $\text{SiO}_2$  involves highly localized silicon “dangling bond” wave function defects. Defects with more delocalized wave functions may dominate the defect structure of high- $\kappa$  dielectrics such as  $\text{HfO}_2$ . One example is the  $\text{O}_2^-$  defect, the precursor to which is likely a dominant electron trap in  $\text{HfO}_2$ . The unpaired electron wave function of the  $\text{O}_2^-$  is less localized than the  $\text{E}'$  center, the

dominant defect in  $\text{SiO}_2$  which has been implicated in TDDDB by some studies. Thus, although atomic distances are similar, the dielectric defect wave functions are likely different and may have larger effective radius than  $\text{E}'$  centers. Although the  $\text{O}_2^-$  defect has not been linked to TDDDB, one might speculate that a possible reason for the persistent low Weibull slopes in high- $\kappa$  films is that the defects involved have a larger effective radius than those involved in breakdown in  $\text{SiO}_2$ .

## VI. CONCLUDING REMARKS

Defect levels at the dielectric/silicon interface, in the dielectric, and possibly also near the dielectric/metal gate, will play dominating roles in determining the performance and reliability of MOS devices that incorporate high- $\kappa$  dielectrics. The few ESR studies that have provided some understanding of these defects have been reviewed. Several independent studies on high- $\kappa$  gate oxides all strongly indicate that Si/dielectric interface silicon dangling bond defects similar to the  $\text{P}_b$  centers of conventional Si/ $\text{SiO}_2$  technology play dominant roles in the Si/dielectric interface traps of these systems. Limited ESR studies of defect centers in the dielectric “bulk” indicate the presence of traps very different from those in  $\text{SiO}_2$ . The differences in the traps will almost certainly be reflected in the response of high- $\kappa$  based MOS technology to a variety of stressing conditions. An understanding of the physical and chemical nature of these defects will likely help process engineers and device designers to eliminate or ameliorate reliability problems caused by these defects.

## ACKNOWLEDGMENT

The authors thank Dr. Y. Ono, Dr. D. Tweet, Dr. W. Zhuang, and Dr. S.T. Hsu of Sharp Labs of America, Prof. R. Solanki of the Oregon Graduate Institute, A. Kang of Penn State University, and Dr. W. Tsai of Intel for high- $\kappa$  research collaborations, Dr. J. Suehle of NIST and Dr. G. Bersuker for valuable technical discussions, and T. Pribicko and J. Ryan for assistance with manuscript preparation.

## REFERENCES

- [1] The International Technology Roadmap for Semiconductors [Online]. Available: <http://public.itrs.org>
- [2] G. D. Wilk, R. M. Wallace, and J. M. Anthony, *J. Appl. Phys.*, vol. 89, p. 5243, 2001.
- [3] K. J. Hubbard and D. G. Schlom, *J. Mater. Res.*, vol. 11, p. 2757, 1996.
- [4] J. Robertson, *J. Vac. Sci. Tech.*, vol. B18, p. 1785, 2000.
- [5] M. Gutowski, J. E. Jaffe, C.-L. Liu, M. Stoker, R. I. Hegde, R. S. Rai, and P. J. Tobin, *Appl. Phys. Lett.*, vol. 80, p. 1897, 2002.
- [6] A. Y. Kang, P. M. Lenahan, and J. F. Conley Jr., *Appl. Phys. Lett.*, vol. 83, no. 16, p. 3407, 2003.
- [7] J. F. Conley Jr., Y. Ono, R. Solanki, G. Stecker, and W. Zhuang, *Appl. Phys. Lett.*, vol. 82, no. 20, p. 3508, 2003.
- [8] S. Zafar, A. Callegari, E. Gusev, and M. V. Fischetti, *IEDM Tech. Dig.*, vol. 2002, 2002, p. 517.
- [9] W. J. Zhu and T. P. Ma, *IEEE Electron Device Lett.*, vol. 23, p. 597, 2002.
- [10] E. P. Gusev, D. A. Buchanan, E. Cartier, A. Kumar, D. DiMaria, S. Guha, A. Callegari, S. Zafar, P. C. Jamison, D. A. Neumayer, M. Copel, M. A. Gribelyuk, H. Okorn-Schmidt, C. D’Emic, R. J. Fleming, A. Mocuta, and A. Ajmera, *IEDM Tech. Dig.*, vol. 2001, 2001, p. 451.
- [11] P. M. Lenahan and J. F. Conley Jr., *J. Vac. Sci. and Tech. B*, vol. 16, p. 2134, 1998.
- [12] J. F. Conley Jr., *Materials Research Society Proc.*, vol. 428, 1996, p. 293.

- [13] Y. Nishi, T. Tanaka, and A. Ohwada, *Jpn. J. Appl. Phys.*, vol. 11, p. 85, 1972.
- [14] E. E. Poindexter, P. J. Caplan, B. E. Deal, and R. R. Razouk, *J. Appl. Phys.*, vol. 52, p. 879, 1981.
- [15] P. J. Caplan, E. H. Poindexter, B. E. Deal, and R. R. Razouk, *J. Appl. Phys.*, vol. 50, p. 5847, 1979.
- [16] P. M. Lenahan and P. V. Dressendorfer, *Appl. Phys. Lett.*, vol. 41, p. 542, 1982.
- [17] —, *J. Appl. Phys.*, vol. 55, p. 3495, 1984.
- [18] Y. Y. Kim and P. M. Lenahan, *J. Appl. Phys. Lett.*, vol. 84, p. 3551, 1988.
- [19] J. T. Krick, P. M. Lenahan, and G. J. Dunn, *Appl. Phys. Lett.*, vol. 59, p. 3437, 1991.
- [20] W. L. Warren and P. M. Lenahan, *Appl. Phys. Lett.*, vol. 49, p. 1296, 1988.
- [21] J. W. Gabrys, P. M. Lenahan, and W. Weber, *Microelectron. Eng.*, vol. 22, p. 879, 1981.
- [22] G. J. Gerardi, E. H. Poindexter, P. J. Caplan, and N. M. Johnson, *Appl. Phys. Lett.*, vol. 49, p. 348, 1986.
- [23] E. H. Poindexter, G. J. Gerardi, M. E. Ruckel, P. J. Caplan, N. M. Johnson, and D. K. Biegelson, *J. Appl. Phys.*, vol. 56, p. 2844, 1984.
- [24] J. P. Campbell and P. M. Lenahan, *Appl. Phys. Lett.*, vol. 80, p. 1945, 2002.
- [25] A. Stesmans, B. Nouwen, and V. V. Afanas'ev, *Phys. Rev. B*, vol. 58, p. 15801, 1998.
- [26] P. M. Lenahan and P. V. Dressendorfer, *IEEE Trans. Nucl. Sci.*, vol. 30, p. 4602, 1983.
- [27] T. Takahashi, B. B. Triplett, K. Yokogawa, B. Kim, K. Osada, and T. Sugano, *Appl. Phys. Lett.*, vol. 50, p. 1334, 1987.
- [28] B. B. Triplett, T. Takahashi, and T. Sugano, *Appl. Phys. Lett.*, vol. 50, p. 1663, 1987.
- [29] L. Lipkin, L. Rowan, A. Reisman, and C. K. Williams, *J. Electrochem. Soc.*, vol. 138, p. 2050, 1991.
- [30] H. Miki, M. Noguchi, K. Yokogawa, B. Kim, K. Asada, and T. Sugano, "Electron and hole traps in SiO<sub>2</sub> films thermally grown on Si substrates in ultra-dry oxygen," *IEEE Trans. Electron. Dev.*, vol. 35, no. 12, pp. 2245–2252, Dec. 1988.
- [31] K. Awazu, W. Watanobe, and H. Kawazoe, *J. Appl. Phys.*, vol. 73, p. 8519, 1993.
- [32] R. L. Vranich, B. Henderson, and M. Pepper, *Appl. Phys. Lett.*, vol. 52, p. 1161, 1988.
- [33] J. F. Conley Jr., P. M. Lenahan, and P. Roitman, "Electron spin resonance study of E' trapping centers in SIMOX buried oxides," *IEEE Trans. Nucl. Sci.*, vol. 38, no. 6, pp. 1247–1252, Dec. 1991.
- [34] —, *Appl. Phys. Lett.*, vol. 60, p. 2889, 1992.
- [35] J. F. Conley Jr., P. M. Lenahan, R. K. Lowry, H. L. Evans, and T. J. Morthorst, *J. Appl. Phys.*, vol. 76, p. 2872, 1994.
- [36] J. McPherson *et al.*, *Appl. Phys. Lett.*, vol. 71, 1997.
- [37] T. Oldham and A. Lelis, *MRS Proc.*, vol. 248, 1996.
- [38] P. M. Lenahan and P. M. Mele, *J. Vac. Sci. Technol. B*, vol. 18, 2000.
- [39] J. F. Conley Jr., P. M. Lenahan, and B. D. Wallace, *IEEE Integrated Reliability Workshop (IRW) Final Report*, 1996, pp. 134–141.
- [40] P. M. Lenahan and J. F. Conley Jr., *J. Appl. Phys.*, vol. 81, p. 6822, 1997.
- [41] J. F. Conley Jr., P. M. Lenahan, B. D. Wallace, and P. Cole, "Quantitative model of radiation induced charge trapping in SiO<sub>2</sub>," *IEEE Trans. Nucl. Sci.*, vol. 44, no. 6, pp. 1804–1809, Dec. 1997.
- [42] P. M. Lenahan and J. F. Conley Jr., *Appl. Phys. Lett.*, vol. 71, p. 3126, 1997.
- [43] A. Stesmans, V. Afanas'ev, and M. Houssa, *J. Noncryst. Sol.*, vol. 303, p. 162, 2002.
- [44] A. Stesmans and V. Afanas'ev, *Appl. Phys. Lett.*, vol. 80, p. 1957, 2002.
- [45] S. Baldovino, S. Nokhrin, G. Scarel, M. Fanciulli, T. Graf, and M. S. Brandt, *J. Non-Cryst. Sol.*, vol. 322, p. 168, 2003.
- [46] E. P. Gusev, C. Cabral Jr., M. Copel, C. D'Emic, and M. Gribelyuk, *Micro. Eng.*, vol. 69, p. 145, 2003.
- [47] M. Alam and M. Green, *J. Appl. Phys.*, vol. 94, p. 3404, 2003.
- [48] J. F. Conley Jr., Y. Ono, and D. J. Tweet, *Appl. Phys. Lett.*, vol. 84, no. 11, p. 1913, 2004.
- [49] A. Y. Kang, P. M. Lenahan, J. F. Conley Jr., and R. Solanki, *Appl. Phys. Lett.*, vol. 81, p. 1128, 2002.
- [50] A. Y. Kang, P. M. Lenahan, and J. F. Conley Jr., "The radiation response of the high dielectric-constant hafnium oxide/silicon system," *IEEE Trans. Nucl. Sci.*, vol. 49, no. 6, pp. 2636–2642, Dec. 2002.
- [51] A. Y. Kang, P. M. Lenahan, J. F. Conley Jr., and Y. Ono, *2003 IEEE Integrated Reliability Workshop Final Report*, p. 24.
- [52] J. F. Conley Jr., Y. Ono, D. J. Tweet, W. Zhuang, and R. Solanki, *J. Appl. Phys.*, vol. 93, p. 712, 2003.
- [53] J. F. Conley Jr., Y. Ono, W. Zhuang, D. J. Tweet, W. Gao, S. K. Mohammed, and R. Solanki, *Electrochem. Solid State Lett.*, vol. 5, no. 5, p. C57, 2002.
- [54] J. F. Conley Jr., Y. Ono, D. J. Tweet, and R. Solanki, *Appl. Phys. Lett.*, vol. 84, no. 3, p. 398, 2004.
- [55] A. Stesmans and V. Afanas'ev, *Appl. Phys. Lett.*, vol. 82, p. 4074, 2003.
- [56] P. M. Lenahan, A. Kang, and J. F. Conley Jr., unpublished.
- [57] T. G. Pribicko, J. P. Campbell, P. M. Lenahan, W. Tsai, and A. Kerber, *Appl. Phys. Lett.*, vol. 86, no. 18, 2005.
- [58] J. L. Cantin and H. J. von Bardeleben, *J. Non-Cryst. Sol.*, vol. 303, p. 175, 2002.
- [59] R. E. Mikawa and P. M. Lenahan, *J. Appl. Phys.*, vol. 59, p. 2054, 1986.
- [60] M. Shiotani, G. Moro, and J. H. Freed, *J. Chem. Phys.*, vol. 74, p. 2616, 1981.
- [61] P. H. Kasai, *J. Chem. Phys.*, vol. 43, p. 3322, 1965.
- [62] X. Zhang and K. J. Klabunde, *Inorg. Chem.*, vol. 31, p. 1706, 1992.
- [63] R. F. Howe and M. Gratzel, *J. Phys. Chem.*, vol. 91, p. 3906, 1987.
- [64] R. F. Howe and W. C. Timmer, *J. Chem. Phys.*, vol. 85, p. 6129, 1986.
- [65] E. Abi-Aad, R. Bechara, J. Grimblot, and A. Aboukais, *Chem. Mater.*, vol. 5, p. 793, 1993.
- [66] J. Matta, J. F. Lamoniér, E. Abi-Aad, E. A. Zhilinskaya, and A. Aboukais, *Phys. Chem. Chem. Phys.*, vol. 1, p. 4975, 1999.
- [67] V. Ramaswamy, B. Tripathi, D. Srinivas, A. V. Ramaswamy, R. Cattaneo, and R. Prins, *J. Catal.*, vol. 200, p. 250, 2001.
- [68] E. Giamello, M. Volante, B. Fubini, F. Geobaldo, and C. Morterra, *Mater. Chem. Phys.*, vol. 29, p. 379, 1991.
- [69] M. Anpo, M. Che, B. Fubini, E. Garrone, E. Giamello, and M. C. Paganini, *Top. Catal.*, vol. 8, p. 189, 1999.
- [70] J. H. Lunsford, *Catal. Rev.*, vol. 8, p. 135, 1973.
- [71] M. Che and A. J. Tench, *Adv. Catal.*, vol. 32, p. 1, 1983.
- [72] W. Kanzig and M. H. Cohen, *Phys. Rev. Lett.*, vol. 3, p. 509, 1959.
- [73] C. Morterra, E. Giamello, L. Orto, and M. Volante, *J. Phys. Chem.*, vol. 94, p. 3111, 1990.
- [74] A. Stesmans, V. V. Afanas'ev, F. Chen, and S. A. Campbell, *Appl. Phys. Lett.*, vol. 84, no. 22, p. 4574, 2004.
- [75] J. C. Lee, S. J. Oh, M. Cho, C. S. Hwang, and R. Jung, *Appl. Phys. Lett.*, vol. 84, no. 8, p. 1305, 2004.
- [76] G. D. Wilk and D. A. Muller, *Appl. Phys. Lett.*, vol. 83, no. 19, p. 3984, 2003.
- [77] G. Bersuker, P. Zeitzoff, G. Brown, and H. R. Huff, *Mat. Tod.*, pp. 26–33, Jan. 2004.
- [78] P. Lysaght, B. Foran, S. Stemmer, G. Bersuker, J. Bennett, R. Tichy, L. Larson, and H. Huff, *Micro. Eng.*, vol. 69, p. 182, 2003.
- [79] D. W. McComb, A. J. Craven, D. A. Hamilton, and M. MacKenzie, *Appl. Phys. Lett.*, vol. 84, p. 4523, 2004.
- [80] T. Kauerauf, R. Degraeve, E. Cartier, C. Soens, and G. Groeseneken, *IEEE Electron Device Lett.*, vol. 23, no. 4, p. 215, 2002.
- [81] Y. H. Kim, K. Onishi, C. S. Kang, H. Cho, R. Choi, S. Krishnan, M. Akbar, and J. C. Lee, *Electron Devices Lett.*, vol. 24, p. 40, 2003.
- [82] R. Degraeve, T. Kauerauf, A. Kerber, E. Cartier, B. Govoreanu, P. Roussel, L. Pantisano, P. Blomme, B. Kaczer, and G. Groeseneken, *Proc. IEEE IRPS 2003*, p. 23.
- [83] Y. Garros *et al.*, *Proc. IEEE IRPS 2004*.
- [84] G. Harada, M. Niwa, S. Lee, and D. L. Kwong, *2002 VLSI Symp. Tech. Dig.*
- [85] D. L. Lee *et al.*, *IEEE Electron Device Lett.*, vol. 25, p. 13, 2004.
- [86] K. Onishi, C. S. Kang, R. Choi, H.-J. Cho, S. Gopalan, R. Nieh, E. Dharmarajan, and J. C. Lee, *IEDM 2001 Tech. Dig.*, p. 659.
- [87] J. Stathis, *J. Appl. Phys.*, vol. 86, p. 5757, 1999.
- [88] R. Degraeve, G. Groeseneken, R. Bellens, J. L. Ogier, M. Depas, and P. J. Roussel, *IEEE Trans. Electron Devices*, vol. 45, no. 4, pp. 904–911, Apr. 1998.
- [89] J. McPherson, J. Y. Kim, A. Shanware, and H. Mogul, *Appl. Phys. Lett.*, vol. 82, no. 13, p. 2121, 2003.
- [90] R. Degraeve, G. Groeseneken, R. Bellens, J. L. Ogier, M. Depas, and P. J. Roussel, *IEEE Trans. Electron Devices*, vol. 45, no. 4, pp. 904–911, Apr. 1998.



**Patrick M. Lenahan** (M'93) received the B.S. degree from the University of Notre Dame, Notre Dame, IN, and the Ph.D. degree from the University of Illinois at Champaign-Urbana in 1979.

He was a Postdoctoral Fellow at Princeton University, Princeton, NJ, in 1979 and 1980. From 1980 to 1985, he was a Member of the Technical Staff in the Materials Research Directorate of Sandia National Laboratories, Albuquerque, NM. Since 1985, he has been at Pennsylvania State University where he is Professor of Engineering Science and

Mechanics. In 2001, he was Visiting Professor of Electronics and Computer Engineering at Nihon University, Tokyo, Japan. From 2000 to 2004, he served as an associate editor of the *Journal of Electronic Materials*. He has authored over 120 publications, approximately 140 conference presentations, and one patent. His research has been primarily focused upon the trapping centers in semiconductors and insulators: amorphous SiO<sub>2</sub>, nitrogen, phosphorous, and boron "doped" SiO<sub>2</sub>, silicon nitrides, silicon oxynitrides, Si/SiO<sub>2</sub> interfaces, silicon grain boundaries and silicon carbide with a variety of electrical measurements and electron spin resonance techniques.



**John F. Conley, Jr.** (S'89-M'91-SM'02) received the B.S. degree in electrical engineering in 1991 and the Ph.D. degree in engineering science and mechanics in 1995 from The Pennsylvania State University, University Park, where he won a 1996 Xerox Prize for his Ph.D. dissertation.

After completion of the Ph.D., he was with Dynamics Research Corporation from 1995 to 2000 and with the Jet Propulsion Laboratory from 2000 to 2001, where he received an achievement award. Since 2001, he has been a Senior Member

of the Technical Staff at Sharp Laboratories of America, Camas, WA, where his research interests include advanced gate stacks, atomic layer deposited high- $\kappa$  dielectrics, and optoelectronic/sensing applications of nano-structured materials. In 2002–2003, he served as an adjunct Professor at the Vancouver campus of Washington State University. He has authored or co-authored over 80 technical papers, over 80 conference presentations, and one U.S. patent with several pending. He has recently presented tutorial short courses on high- $\kappa$  dielectrics at the 2004 IEEE International Reliability Physics Symposium and the 2004 IEEE Integrated Reliability Workshop.

In addition to co-editing this IEEE TRANSACTIONS ON DEVICE AND MATERIALS RELIABILITY special issue on High- $\kappa$  Reliability, Dr. Conley has served on the technical committees of the IRPS, the SOI Conference, and the Nuclear and Space Radiation Effects Conference, and was technical program chair of the 2000 IEEE Microelectronics Reliability and Qualification Workshop. He is currently serving as the technical program chair of the 2005 IEEE International Integrated Reliability Workshop.